Non-monotonic Size Dependence of Electron Mobility in Indium Oxide Nanocrystals Thin Film Transistor

Hien Thu Pham and Hyun-Dam Jeong[*]

Department of Chemistry, Chonnam National University, Gwangju 500-757, Korea. [*]E-mail: hdjeong@chonnam.ac.kr

Indium oxide nanocrystals (In_2O_3 NCs) with sizes of 5.5 nm–10 nm were synthesized by hot injection of the mixture precursors, indium acetate and oleic acid, into alcohol solution (1-octadecanol and 1-octadecene mixture). Field emission transmission electron microscopy (FE-TEM), High resolution X-Ray diffraction (X-ray), Nuclear magnetic resonance (NMR), and Fourier transform infrared spectroscopy (FT–IR) were employed to investigate the size, surface molecular structure, and crystallinity of the synthesized In_2O_3 NCs. When covered by oleic acid as a capping group, the In_2O_3 NCs had a high crystallinity with a cubic structure, demonstrating a narrow size distribution. A high mobility of 2.51 cm²/V·s and an on/off current ratio of about 1.0×10^3 were observed with an In_2O_3 NCs thin film transistor (TFT) device, where the channel layer of In_2O_3 NCs thin films were formed by a solution process of spin coating, cured at a relatively low temperature, 350 °C. A size-dependent, non-monotonic trend on electron mobility was distinctly observed: the electron mobility increased from 0.43 cm²/V·s for NCs with a 5.5 nm diameter to 2.51 cm²/V·s for NCs with a diameter of 7.1 nm, and then decreased for NCs larger than 7.1 nm. This phenomenon is clearly explained by the combination of a smaller number of hops, a decrease in charging energy, and a decrease in electronic coupling with the increasing NC size, where the crossover diameter is estimated to be 7.1 nm. The decrease in electronic coupling proved to be the decisive factor giving rise to the decrease in the mobility associated with increasing size in the larger NCs above the crossover diameter.

Key Words : Indium oxide nanocrystals, Thin film transistor, Electron mobility, Non-monotonic, Electronic coupling

Introduction

A great deal of focus on metal oxide semiconductors has been observed in recent years as a means of realizing transparent electronics for next generation display applications; such materials are expected to enable the realization of transparent pixel transistors for display that do not block light, enabling realization of brighter displays with a higher aperture ratio. Among them, indium oxide (In_2O_3), an n-type metal oxide semiconductor, has attracted much attention because of its wide bandgap (direct bandgap around 3.6 eV at room temperature), high single crystal mobility (160 cm²/V·s), and good visible region transparency (> 90%).[1] Previous studies have mainly focused on the fabrication of In_2O_3 thin films using sputtering, spray pyrolysis, and chemical vapor deposition methods.[2-4] The In_2O_3 thin films deposited using sputtering have exhibited field-effect mobilities (m) as high as 130 cm²/V·s, $I_{on}/I_{off} = 10^5$, subthreshold gate voltage swing (S.S.) = 190 mV/decade.[4]

More recently, Marks *et al.* first reported in 2008 a solution-processed In_2O_3 thin film transistor (TFT), where the In_2O_3 semiconducting channel layer was formed from an indium chloride ($InCl_3$) precursor solution by a spin coating process, producing a high mobility value (~43 cm²/V·s) and an excellent TFT performance ($I_{on}/I_{off} = 10^6$) at the annealing temperature of about 400 °C.[5] In 2011, Marks *et al.* reported in improvement, the low-temperature (325 °C) fabrication of

high-performance solution-processed In_2O_3 TFT ($\mu = 9.4$ cm²/V·s; $I_{on}/I_{off} = 10^3$) with combustion processing.[6] In 2011, Bae *et al.* reported a solution-processed In_2O_3 thin film transistor (TFT), with indium acetyacetonate ($In(acac)_3$) as an indium source precursor, achieving a high TFT performance ($\mu = 2.37$ cm²/V·s; $I_{on}/I_{off} = 10^6$) at an annealing temperature of 250 °C.[7] The same group also reported a simple and novel aqueous route for the fabrication of indium oxide TFTs at a low annealing temperature (200 °C) using unique indium complex ($In(OH_2)_6^{3+}$), which was converted from indium nitrate ($InNO_3$) in water solvent, with post annealing on both SiO_2 and flexible plastic substrates.[8] The metal oxide TFTs fabricated showed good device uniformity and good electrical performance: $\mu = 2.62 \pm 0.25$ cm²/V·s and S.S. $= 0.29 \pm 0.06$ V/decade, with a turn-on voltage of 0 V for SiO_2 substrates; $\mu = 3.14$ cm²/V·s, S.S. $= 158$ mV/decade and $I_{on}/I_{off} > 10^9$ for the flexible PEN substrate.[8] Continuous investigations by the group uncovered a novel material using fluorine-doped indium zinc oxide (IZO:F) flexible TFTs, which showed that fluorine doping can enhance the mobility and improve the gate bias stability of TFT ($\mu = 6.4$ cm²/V·s; $I_{on}/I_{off} = 10^8$) which was fabricated at the annealing temperature of 200 °C.[9]

Even though there have been a lot of studies on solution-processed In_2O_3 TFT, including ones mentioned above,[1-13] the investigation of thin films of In_2O_3 nanocrystals (NCs) using solution-processing deposition, and its applications
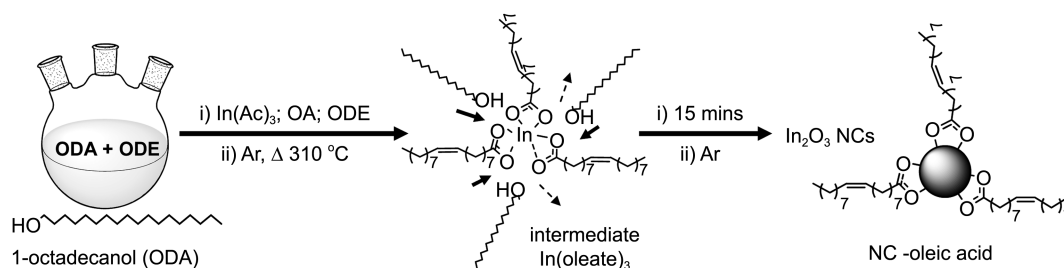
Scheme 1. Synthetic procedure for indium oxide NCs (NCs–oleic acid). The fast injection of indium oleate precursor into alcohol solution (ODA in ODE solvent) at high temperature (310 °C) during 15 mins resulted in indium oxide NCs formation.

into the solution-processed TFT, have rarely been performed. In this article, we report the preparation of colloidal, highly crystalline In$_2$O$_3$ NCs with a defined size controllability of by use of the hot injection method, and its applications in the channel layer of In$_2$O$_3$ NCs TFTs. There are two fundamental motivations for the utilization of In$_2$O$_3$ thin films: (i) the prefect nanocrystalline domain inside the NCs is believed to endow a high intrinsic mobility in the finally deposited NCs thin films; (ii) The NCs thin film is one of the best solid material systems for validation of the concept of artificial solids[14,15] in a practical manner. The electron transport properties of the artificial solids are known to be controlled by changing the size of the building block and interdistance between them.[14,16] In the In$_2$O$_3$ NC thin films, the size and interdistance of the NCs are easily determined by the synthetic conditions and capping ligands, respectively. Our In$_2$O$_3$ NCs were capped with oleic acid (Schematic 1), and we used spin-coated In$_2$O$_3$ NCs film to successfully fabricate high-performance In$_2$O$_3$ TFT at a low curing temperature (350 °C) giving the excellent mobility of about 2.51 cm^2/V·s. Interestingly, we also found that the electron mobility was non-monotonically dependent on the size of In$_2$O$_3$ NCs; the electron mobility increased from 0.43 cm^2/V·s for NCs with a 5.5 nm diameter to 2.51 cm^2/V·s for NCs with a 7.1 nm diameter (Region 1), dropping off for larger NCs (Region 2). The decreasing charging energy E$_C$ in region 1 (d ≤ 7.1 nm), and the smaller number of hops needed for carriers to travels across channels composed of a lager size were mainly considered for the monotonically increase of mobility. On the other hand, region 2 (d > 7.1 nm) displayed a decrease in mobility with an increase in size, resulting from the degeneration of coupling energy E$_V$.

Experimental

Materials. The chemicals used included Indium (III) acetate (In(Ac)$_3$, 99.99%, Aldrich), Oleic acid (C$_{17}$H$_{34}$COOH; OA, 95% Aldrich), 1-octadecanol (C$_{18}$H$_{37}$OH; ODA, 97% Alfa Aesar), and 1-octadecene (C$_{18}$H$_{36}$; ODE, 90% Aldrich). All chemicals were used without further purification.

Synthesis of Stable Dot-shaped In$_2$O$_3$ Nanocrystals. The In$_2$O$_3$ NCs were synthesized using established methods by Narayanaswamy *et al.*, with the modifications.[17] Stable dot-shaped (5–10 nm) In$_2$O$_3$ nanocrystals were formed by direct injection of the precursors solution into three-neck

flask which contained alcohol solution. Briefly, the alcohol solution containing ODA (8.7 g) and ODE (75 mL) were load in a 250 mL three-necked flask, degassed at 120 °C for 2 h, then heated to 310 °C. Then a typical solution precursor containing indium (III) acetate, and oleic acid in 7.5 mL of ODE were prepared separately by degassing and heating to 120 °C, then swiftly injected into the above alcohol solution at 310 °C. When the temperature of the resulting mixture dropped to about 294 °C, it was incubated for 15 mins. The mixture was cooled to 50 °C, then acetone was used to quench the reaction and precipitate the entire product, and the nanocrystals were collected by centrifugation. The nanocrystals were then dispersed in hexane, and any insoluble residue was removed by centrifugation. Purification was performed by washing several times with hexane and acetone. The NCs were vacuum-dried for 12 h at 100 °C. A slightly yellow powder was collected and dissolved well in various organic solvents.

The preparation of indium oxide nanocrystals in ODE with different In:OA molar ratios, 1:1, 1:3, 1:5, 1:6, 1:7, and 1:8 as mention in Table 1 have given a different size of NCs. Excepting the changing in the molar ratio between In:OA, all condition synthesis and the purification steps were the same as those described above.

Preparation of NC Films. Thin film transistor (TFT) device was fabricated in standard bottom-gate, top contact configuration. Nanocrystal solution with an approximate concentration of 3 wt % in toluene solvent was spin coated on a SiO$_2$ (100 nm)/Si substrate. The doped silicon wafer acted as the gate electrode. After spinning, the samples were covered in aluminum foil and soft-annealed at 80 °C for 1 hour, then hard-annealed at 350 °C in ambient air conditions. A 100 nm thick aluminum layer was deposited through a shadow mask for the source and drain contacts.

Material Characterization. Field emission transmission electron microscopy (FE-TEM) images of samples were taken using a JEOL JEM-2100F, operated at 80-200 kV. Field emission scanning electron microscopy (FE-SEM) images of samples were taken using a JEOL ISM-7500F, operated at 15 kV. For TEM sampling, one drop of a solution of 0.2 wt % of In$_2$O$_3$ NCs on toluene was casted onto a graphite-coated copper grid and then dried in a vacuum overnight. High resolution X-Ray diffractometer images were collected using a X'Pert PRO Multi Purpose X-Ray diffractometer with a Cu Kα source, operated at 40 kV and 30 mA. The 2θ

Table 1. Summary of synthesized condition and electric properties of NCs raging from 5.5–10.0 nm: mobility value μ, threshold voltage (V_T), and on and off current ratio (I_{on}/I_{off}))

NCs Diameter [nm]	ODA [gram]	ODE [mL]	In:OA [molar ratio]	$In(Ac)_3$ [gram][a]	OA [gram][a]	Mobility [$cm^2 \cdot V^{-1} \cdot s^{-1}$]	V_T [V]	$I_{on/off}$
5.5 nm	8.7	75	1:3	0.43	1.27	0.43 ± 0.03	−17.9 ± 4.8	8.3×10^2
6.8 nm	8.7	75	1:5	0.43	2.11	1.14 ± 0.07	−17.4 ± 2.1	4.3×10^2
7.1 nm	8.7	75	1:6	0.43	2.54	2.51 ± 0.14	−22.3 ± 3.5	2.0×10^3
7.8 nm	8.7	75	1:7	0.43	2.96	1.35 ± 0.19	−26.6 ± 4.6	7.1×10^2
10 nm	8.7	75	1:8	0.43	3.38	0.44 ± 0.09	−25.1 ± 4.0	3.1×10^2

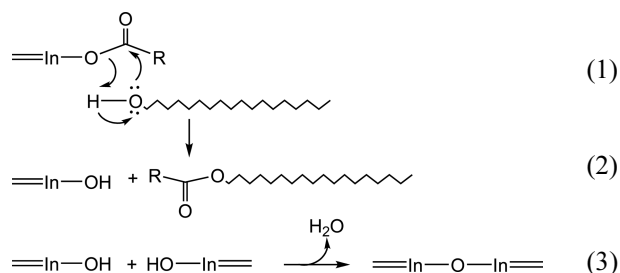[a]$In(Ac)_3$ and OA was prepared in the presence of 7.5 mL ODE

angle was scanned from 10° to 90°. Fourier transform infrared spectroscopy (FT-IR) was performed on a spectrum 400 (PekinElmer, USA). All NMR data were collected on the FT-NMR 300 MHz (Varian Inc, Palo Alto, California, USA). Chemical shifts were reported in parts per million (ppm) and toluene-d_8 was used as a solvent. Thermogravimetric (TG) analysis was conducted on a TGA-50H under air condition flow in a range from room temperature to 900 °C. TFT properties were analyzed on an HP4145B semiconductor analyzer with gate voltage (VG) limited to 40 V (from –40 V to +40 V).
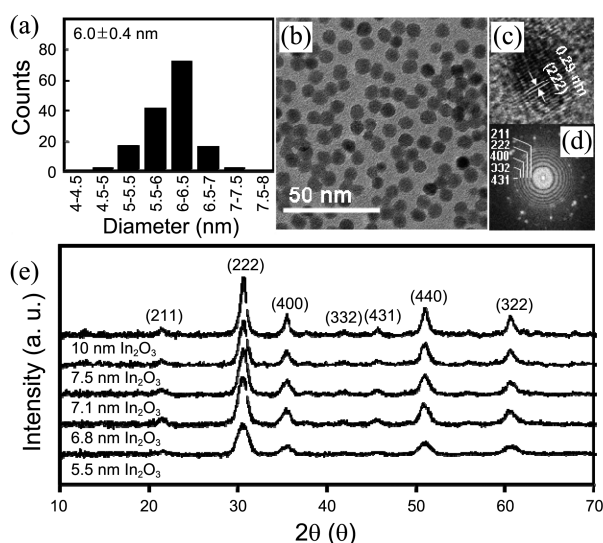
Results and Discussion

The oleic acid capped In_2O_3 NCs were synthesized by direct injection of the indium oleate precursor ($In(OA)_3$) in 1-octadecene (ODE) into a 1-octadecanol solution (ODA) at a high temperature (310 °C) (see experimental section).[17-19] The typical reaction was summarized in schematic 1. To tune the size of the NCs, reaction conditions were modified, as summarized in Table 1. This resulted in the successful synthesis of In_2O_3 NCs with sizes, as follows: 5.5 nm, 6.8

Figure 1. (a) Sizing histograms, (b) TEM image, (c) TEM image of one NC, (d) a selected area electron diffraction pattern (SAED) of 5.5 nm In_2O_3 NCs and (e) XRD patterns of 5.5 nm In_2O_3 NCs, 6.8 nm In_2O_3 NCs, 7.1 nm In_2O_3 NCs, 7.5 nm In_2O_3 NCs, and 10 nm In_2O_3 NCs.

nm, 7.1 nm, 7.5 nm, and 10 nm, estimated from the XRD results (Fig. 1(e)). The size distribution of the smallest In_2O_3 NCs sample was 6.0 ± 0.4 nm, presented in Figure 1. TEM images of single NCs had a plan distance of 0.29 nm, corresponding to the d-spacing of the (222) planes of cubic In_2O_3 (Fig. 1(c)) The selected area electron diffraction pattern (SAED) was consistent with the cubic structure of In_2O_3, featuring strong ring patterns assigned to (211), (222), (400), (332), and (431) planes, proving the high crystallinity of the NCs (Fig. 1(d)).[17-19] These data referred well with the data of the smallest NCs (5.5 nm NCs) obtained in the XRD pattern (Fig. 1(e)). Figure 1(e) showed an X-ray diffraction of five typical size: 5.5 nm, 6.8 nm, 7.1 nm, 7.5 nm and 10 nm, corresponding well to the cubic phase of In_2O_3 in the standard data (JCPDS 06-0416).[17-19] The crystal size calculated using the Scherer equation was 5.5 nm for the smallest NCs, which is considered to be in good agreement with the observed results from the TEM images of the crystal.
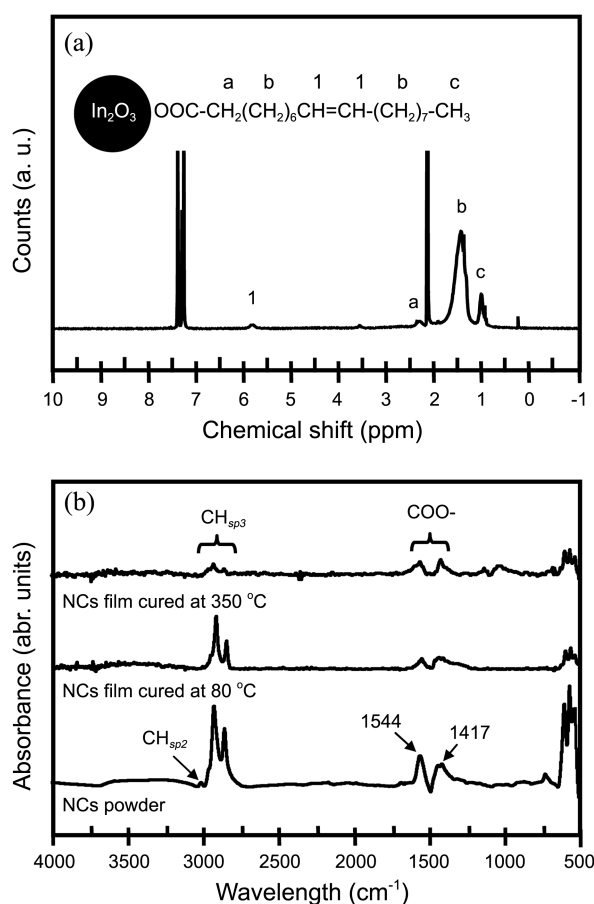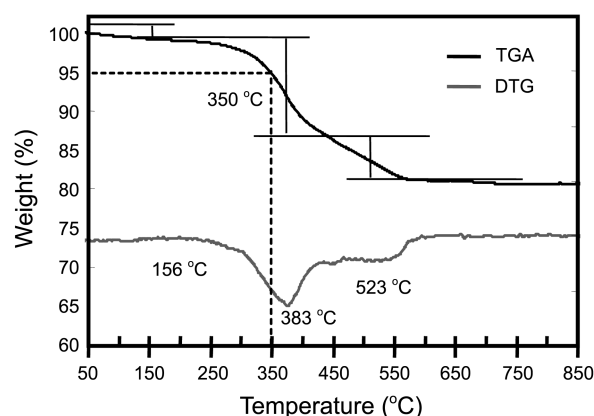
The NMR spectrum of the smallest NCs in toluene solvent showed the appearance of the corresponding proton at 5.6 ppm for (-HC=CH-), 2.3 ppm for (-CH_2-) near the carboxylic group, and 1.4 ppm and 0.99 ppm for the (-CH_2-) and (-CH_3) in the alkyl chain, respectively (Fig. 2(a)). The integral ratio of the (-CH_2-) and (-CH_3) in the alkyl chain is around 7.8/1. Thus, our suggestion of the main reaction observed in this given system is summarized as below:

(1)

(2)

(3)

The ester elimination process used in this study has been employed for the synthesis of metal oxide nanocrystal,[20] such as copper oxide NCs, and zinc oxide NCs.[17,20,21] As shown in the reaction (1)–(3), the In (III) ion, which withdraws electron density from the carboxylate ligand, facilitates the nucleophilic attack of oxygen in 1-octadecanol to the carboxylate ligand, thereby activating the ester elimination reaction.[20-22] The notation R can be understood as the –CH_3 group (from acetic acid) or $CH_3(CH_2)_7CH=CH(CH_2)_6CH_2$-
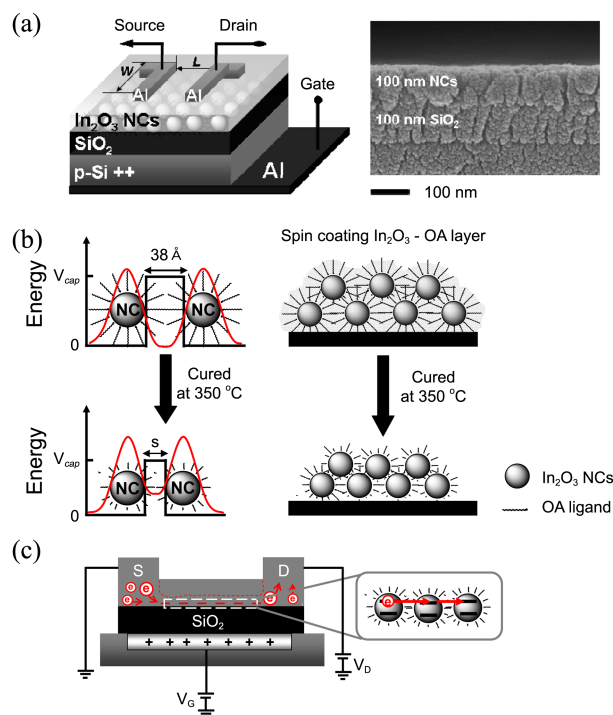
Figure 2. (a) ^{1}H-NMR spectra (300 MHz; toluene-d_8) of 5.5 nm In$_2$O$_3$ NCs. (b) FT-IR spectra of 5.5 nm In$_2$O$_3$ NCs powder, film cured at 80 °C and film cured at 350 °C for the same NCs.

Figure 3. Thermagravimetric analysis–TGA and DTG for In$_2$O$_3$ NCs. TGA runs were conducted at a constant heating rate of 10 °C/min in air. Heating process was carried out up to 900 °C.

Figure 4. (a) Schematic structure and cross-SEM image of the p-Si^{++}/SiO$_2$/NC film cured at 350 °C/Al source-drain TFT device. Channel width (*W*) and channel length (*L*) ratio was 10/1 (b) Schematic structure of NCs channel layer on Si substrate before and after annealing at 350 °C for 3 h (right) and relative schematic representation of their coupling energy diagram (left) before and after annealing; after curing, interdot distance was smaller than 3.8 nm (s < 3.8 nm) producing a higher coupling energy. (c) the *n*-channel semiconductor NCs TFT operator under high fields V$_G$ > 0 and V$_D$ > 0.

group (from oleic acid). Therefore, we proposed the structure of ligand capping on the surface of In$_2$O$_3$ NCs was (CH$_3$(CH$_2$)$_7$CH=CH(CH$_2$)$_6$CH$_2$COO)$_X$(CH$_3$COO)$_{3-X}$. By comparing the integral ratio of (-CH$_2$-) and (-CH$_3$) obtained above (7.8/1) with the ratio of the total relative hydrogen in the two (26x/9) (Fig. 2(a)), the x value was estimated to be 2.7, therefore demonstrating that the ratio between oleic acid and acetic acid on In$_2$O$_3$ NCs surface was 90/10. This means that the surface of In$_2$O$_3$ NCs obtained was mainly covered with oleic acid (OA). Figure 2(b) showed the FT-IR spectra of the 5.5 nm In$_2$O$_3$ NCs powder and In$_2$O$_3$ NCs thin film cured at 80 °C and 350 °C, producing absorption peaks in the range of 3009 cm^{-1}, 2800-3000 cm^{-1} which coincide with the spectrum signals for alkenyl C-H stretch (–HC=CH–) and alkyl C-H stretch (–CH$_3$), respectively. The (COO–) asymmetric vibration band was presented at 1544-1417 cm^{-1}. With the thin films results, it was observed that the majority of the organic ligand on the surface of the thin film was removed after being heated to 350 °C for 3 h.

The organic content of the In$_2$O$_3$ NCs was determined by thermogravimetric analysis (TGA). TGA runs were conducted at a constant heating rate of 10 °C/min in air. The heating process was carried out up to 900 °C, which has been demonstrated to be sufficiently high to degrade all surface bonded molecules, resulting in the thermograms in Figure 3. The weight retention profile was observed to reach a plateau at ~600 °C, confirming that there was no organic material remaining on the In$_2$O$_3$ NCs. From the DTG curves, it could be suggested that the decomposition of remaining acetic acid and water occurred in the period from room temperature up to 156 °C (confirmed by the small percent-
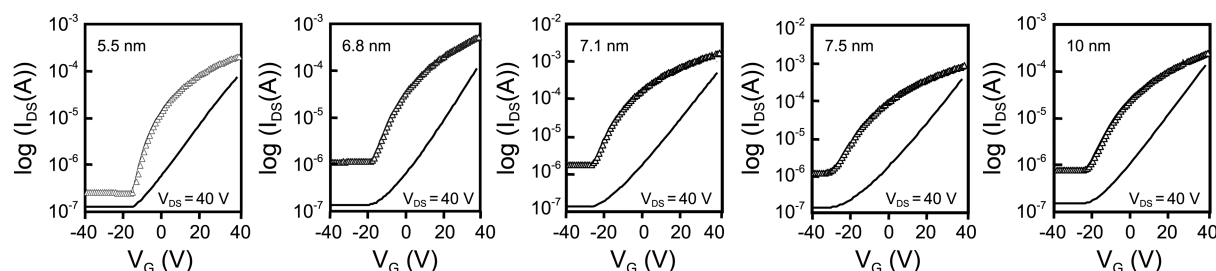
Figure 5. Transfer curve of five TFT device (V_{DS} = 40 V), with NCs size in the following order: 5.5 nm NCs, 6.8 nm NCs, 7.1 nm NCs, 7.5 nm NCs and 10 nm NCs. Volt gate V_G was limited to 40 V (from −40 to 40 V).

age of lost weight, around 3%). This was followed by decomposition of OA ligand, from 156 °C to approximately 523 °C, expressed as a 20% reduction of the weight percentage.

In order to explore the applicability of the In_2O_3 NCs into TFT devices, TFT devices with a structure of p-Si^{++}/SiO$_2$/NC film/Al source-drain were fabricated using a thin film of the NCs on the SiO$_2$/p-Si^{++} substrate cured at 350 °C. The structure of these TFT was schematically shown in Figure 4(a). Thickness of the SiO$_2$ and In_2O_3 NCs film with a crystal size of 5.5 nm were determined by cross-sectional SEM to be about 100 nm and 100 nm, respectively. Five TFT devices with a structure of p-Si++/SiO$_2$/NCs film/Al source-drain were fabricated for comparison. NCs films used as channel layer were made from the crystal sizes of 5.5 nm, 6.8 nm, 7.1 nm, 7.5 nm, and 10 nm. Figure 4(b) shows a schematic representation of the proposed structure of the channel In_2O_3 NCs layer on Si substrate, before and after the films were cured, corresponding to the schematic coupling energy diagram showing the respective differences. After curing, the thickness of the NCs layer was suggested to be decreased, and the films underwent structural variation as depicted. As schematically drawn, the interdistance before curing was estimated to be 38 Å, while the surfaces of the two adjacent NC were separated by 2 times the oleic acid (OA) length. OA length was geometrically optimized by using the Gaussian 03 package at B3LYP level and 6–31** basic set. After curing, the new interdistance generated, which is denoted s, was suggested to be smaller than 38 Å because of the significant removal of the organic capping groups. This reduction of the interdistance lead to a higher electron exchange coupling and increased electron mobility, as depicted in the schematic representation of their coupling energy diagram before and after curing.

To explain further surface structure information, we come back to the simultaneous FT-IR spectra (Fig. 2(b)). Complementary FT-IR spectra of In_2O_3 NCs films deposited on silicon wafer were obtained under 3 h annealing temperatures at 80 °C and 350 °C. At 80 °C, the carboxylic group (COO-), alkenyl C-H stretch (C^{sp2}-H) group and alkyl C-H stretch (C^{sp3}-H) group dominantly appeared on the surface. After the films were cured at 350 °C, most of the organic groups were removed *via* decomposition as we can see in the intensity of peaks. This means that the oleic acid group still remained on surface of NCs, even after curing at 350 °C, as

depicted in Figure 4(b). Figure 4(c) depicted the electron transport in the main channel current of a TFT device under high fields.

Transfer curves was studied by sweeping V_G from −40 to +40 V at V_{DS} = 40 V (Figure 5), for those devices which exhibited the *n*-channel TFT characteristic. The saturated mobility (μ_{sat}) for TFT saturated regions was calculated by fitting a straight line to the plot of the square rot of I_{DS} and V_G, according to the expression: $I_{DS} = (C_i\mu_{sat}.W/2L)(V_G − V_T)^2$, where I_{DS} is the drain current, *W* and *L* are the channel width and length, respectively, μ_{sat} is the field-effect mobility, C_i is the capacitance per unit area, and V_T is the threshold voltage. Value of mobility (μ), threshold voltage (V_T), and I_{on}/I_{off} ratio for those TFT devices were calculated and summarized in Table 1. Briefly, by comparison of the mobility of these films, we obtained significant mobility values reaching 2.5 ± 0.14 (cm^2/V·s), with V_T, and I_{on}/I_{off} were −22 ± 3.5 (V) and 2 × 10^3, respectively for In_2O_3 NCs size of about 7.1 nm. After the diameter of the NCs increased over 7.1 nm to 7.5 nm, a decreased in mobility of 1.5 times was observed, down to 1.35 ± 0,19 (cm^2/V·s). A more dramatic decreased of 5 times was observed when the diameter reached 10 nm, providing a value of 0.44 ± 0.09 (cm^2/V·s). Evidently, the mobility was non-monotonically dependent on the size of NCs.

Figure 6 showed the changes in the electrical parameters such as on and off current based on the diameter of the NCs. Threshold voltage value (Table 1) in our devices were
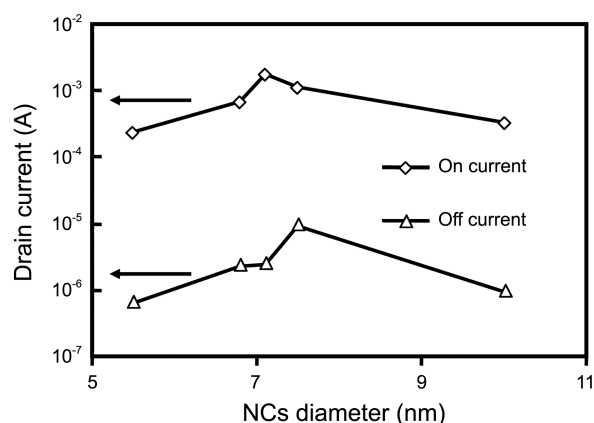
Figure 6. Size dependent on and off current. The off current state was ~10^{-6} to 10^{-5} and the on current state was 10^{-3} to 10^{-2}.

situated in a minus value; the off state (Figure 6) stayed in the range of approximately of 10^{-6} to 10^{-5}, which was quite high compared with the off state for amorphous In_2O_3 previously reported (Marks *et al.*: ~10^{-11};[5,6] Han *et al*: ~10^{-9} [23]). This demonstrates that there are an excess of free electrons for electrical conduction in our NCs films. The main factor controlling the excess of free electrons was the well known oxygen vacancy. The electron was generated easily from oxygen vacancy accrding to the following equation: $O_o^x \rightarrow 1/2 O_2 + V_o^{\cdot\cdot} + 2e^-$ (**3**). The generation of a doubly-charged oxygen vacancy ($V_o^{\cdot\cdot}$) and two free electrons is accelerated by the temperature from the oxide lattice (O_o^x).[9,23,24] In particular, decreasing the off-state current (I_{off}) and controlling the shift of V_T to a positive value by suppressing the generation of oxygen vacancy is crucial for enhancing the electrical properties of our In_2O_3 NCs.[23-25] It should be possible to alter V_T and decrease I_{off} state *via* control of oxygen vacancy through optimized annealing, and modification of the initial material (for example: doping Ga, Zn). In addition, the use of high-K electrics to reduce operating voltage has been widely applied to these semiconductor oxide systems.[4,5,9,26,27]

Previously, Sim *et al.*[26] and Matt *et al.*[27] reported the non-monotonic behavior of electron mobility with a change in PbSe NCs size. This behavior was again explained by investigating three factors: the number of hops, charging energy (E_C) and electronic coupling (E_V). Figure 7(a) showed the charging energy (E_C) and the coupling energy (E_V) of PbSe NCs, which was calculated from the double quantum-well model as a function of NC size.[26] From the experimental data, PbSe NCs mobility was separated to two regions. Region (I) showed an increase in mobility correspondent to an increase in size, where the diameter (d) of NCs is less than 6 nm (d < 6 nm). Region (II) showed a decrease in mobility corresponding to an increase in size, where d is greater than 6 nm (d > 6 nm). Clearly, both the E_C (blue dot line) and E_V (red dot line) decrease with the growing size of NCs, which conflict with each other. In region (I), the E_V was ruled out, and the decreasing charging energy E_C and the smaller number of hops needed for carriers to travels across a channel composed of the lager size were mainly considered for the monotonically increase of mobility. On the other hand, in region (II) the number of hops and charging energy was negligible, instead showing that the coupling energy E_V was a more decisive factor for controlling the mobility. In other words, the decrease of mobility in region (II) was due to the smaller electronic coupling energy. Sim *et al.* used the characteristic crossover diameter (NC size) concept to determine the transition point whereby the role of the number of hops, charging energy, and electronic coupling being responsible for the mobility are changed. Consequently, the crossover diameter of PbSe NCs was estimated to be 6.1 nm, indicating that, for the case with d > 6 nm, the decrease in the electronic coupling was found to deteriorate the electron mobility. This phenomenon was observed with case of In_2O_3 NCs with NC sizes ranging from 5.5 nm to 10 nm The implied crossover diameter was 7.1 nm, where the electron
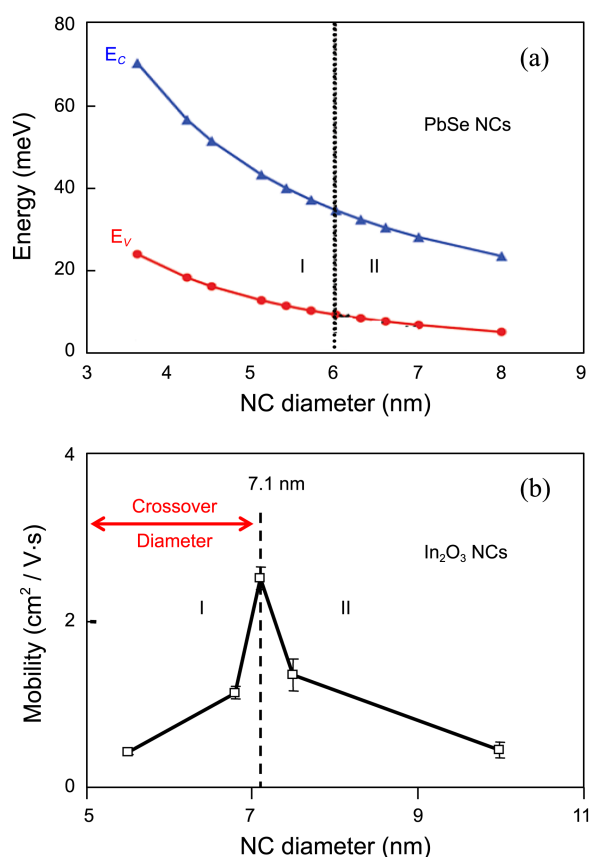
Figure 7. (a) Size dependent charging energy (E_C) along with electronic coupling (E_V) of PbSe NCs; Region I was defined where the diameter of NCs was ≤ 6 nm, whereas region II was defined where the diameter of NCs was > 6 nm, according to reference 8. (b) Size dependent mobility of In_2O_3 NCs; Region I was defined where diameter d ≤ 7.1 nm, whereas region II was defined where d > 7.1 nm. Crossover diameter was estimated to be 7.1 nm.

mobility increased up to a value of 2.51 cm²/V·s before showing a drop off in mobility.

In the consideration of chemically synthesized NCs for electronic applications, the properties of ligand length, size, shape of NCs, and composition of individual NCs have been explored as the building blocks for thin film transistors. As we know, OA capping allows the NCs to form a stable colloidal solution; however, a highly insulating layer of bulky ligands is formed on the surface of the NCs, which displays poor charge transport properties due to weak exchange coupling. In 2005, Talapin *et al.* first reported PbSe NCs capped with oleic acid as a starting material. The NCs film showed to be very insulating, with a conductivity of σ ≈ 10-10 S·cm⁻¹.[28] In this study, we started with monodisperse In_2O_3 capped oleic acid NCs with a well-controlled size and interdistance between NCs. In_2O_3 NCs thin film was cured at 350 °C, and its field-effect mobility was found to be significantly affected by the change in size of the NCs, showing an electron mobility of about 2.51 cm²/V·s for NCs of 7.1 nm in size. Thus, the OA ligand used in this study was considered to be the main factor that inhibited the transport properties of our NCs thin film. The interdistance between NCs has not

been investigated yet in this paper; the ligand exchange process for shorter ligands was expected to significantly enhance the interaction between NCs, and improve the conductivity of NC solid. This issue will be further investigated with more controlled experiments in a separate study.

Conclusion

In summary, i) we have demonstrated the formation of In_2O_3 nanocrystals with sizes ranging from 5.5–10 nm. Oleic acid was found to be the main coverage on the surface of the NCs (Oleic acid 90%). ii) Oleic acid capped indium oxide nanocrystals (In_2O_3–OA NCs) thin films were fabricated by the spin-coating process, then cured at 350 °C for 3 h, showing a high-mobility TFT performance above 2.5 cm^2/V·s mobility, and ~10^3 on off current ratio (I_{on}/I_{off}). Our material was considered to greatly enhance the mobility exhibited by these devices for solution-processed indium oxide NCs on SiO_2 substrate. iii) Interestingly, non-monotonic behavior of electron mobility with the In_2O_3 NCs size was observed: the electron mobility increased from 0.43 cm^2/V·s for NCs with a 5.5 nm diameter to 2.51 cm^2/V·s for NCs with a 7.1 nm diameter, dropping off after that for larger NCs. The decreasing charging energy E_C and the smaller number of hops was used to explain the enhanced mobility along with the size increase up to 7.1 nm Furthermore, the decrease in mobility as the size was increased further was due to the smaller coupling energy E_V. The crossover diameter where electron mobility reached its maximum varies was about 7.1 nm.

References

1. (a) Nakazawa, H.; Ito, Y.; Matsumoto, E.; Adachi, K.; Aoki, N.; Ochiai, Y. J. *Appl. Phys*. **2006**, *100*, 093706. (b) Gupta, A.; Cao, H.; Parekh; Rao, K. K. V.; Raju, A. R.; Waghmare, U. V. J. *Appl. Phys*. **2007**, *101*, 09N513.
2. (a) Murray, C. B.; Norris, D. J.; Bawendi, M. G. *J. Am. Chem. Soc*. **1993**, *115*, 8706. (b) Trindade, T.; O'Brien, P.; Pickett, N. L. *Chem. Mater*. **2001**, *13*, 3843.
3. (a) Ginley, D. S.; Bright, C. *Mater. Res. Soc. Bull*. **2000**, *25*, 15. (b) Chopra, K. L.; Major, S.; Pandya, D. K. *Thin Solid Films* **1983**, *102*, 1. (c) Dawar, A. L.; Joshi, J. C. *J. Mater. Sci.* **1984**, *19*, 1.
4. (a) Wang, L.; Yoon, M.-H.; Facchetti, A.; Marks, T. J. *Adv. Mater*. **2007**, *19*, 3252. (b) Wang, L.; Yoon, M.-H.; Lu, G.; Yang, Y.; Facchetti, A.; Marks, T. J. *Nat. Mater*. **2006**, *5*, 893.
5. Kim, H.-S.; Byrne, P.-D.; Facchetti, A.; Marks, T. J. *J. Am. Chem. Soc*. **2008**, *130*, 12580.
6. Kim, M.-G.; Kanatzidis, M. G.; Facchetti, A.; Marks, T. J. *Nature Material*. **2011**, *10*, 382.
7. Hwang, Y.-H.; Jeon, J.-H.; Bae, B.-S. *Electrochemical and Solid-State Lett.* **2011**, *14*, H303.
8. Hwang, Y.-H.; Seo, J.-S.; Yun, J. M.; Park, H.-J.; Yang, S.-Y.; Park, S.-H. K.; Bae, B.-S. *NPG Asia Materials* **2013**, *5*, e45.
9. Seo, J.-S.; Jeon, J.-H.; Hwang, Y.-H.; Park, H.-J.; Ryu, M.; Park, K. S.-H.; Bae, B.-S. *Scientific Report*. **2013**, *3*, 2085.
10. Dhannanjay, Chu, C.-W. *Appl. Phys. Lett*. **2007**, *91*, 132111.
11. Nilsen, O.; Balasundaraprabhu, R.; Monakhov, E. V.; Muthukumarasamy, N.; Fjellvag, H.; Svensson, B. G. *Thin Solid Films* **2009**, *517*, 6320.
12. Adurodija, F. O.; Izumi, H.; Ishihara, T.; Yoshioka, H.; Matsui, H.; Motoyama, M. *Appl. Phys. Lett*. **1999**, *74*, 3059.
13. Jeong, S.; Ha, Y.-G.; Moon, J.; Facchetti, A.; Marks, T. J. *Adv. Mater*. **2010**, *22*, 1346.
14. Hanrath, T. *J. Vac. Sci. Technol. A* **2012**, *30*, 030820.
15. Beloborodov, I. S.; Lopatin, A. V.; Vinokur, V. M. *Rev. Mod. Phys*. **2007**, *79*, 469.
16. Talapin, D. V.; Lee, J.-S.; Kovalenko, M. V.; Schevchenko, E. V. *Chem. Rev*. **2010**, *110*, 389.
17. Narayanaswamy, A.; Xu, H.; Pradhan, N.; Kim, M.-S.; Peng, X. *J. Am. Chem. Soc*. **2006**, *128*, 10310.
18. Ye, E.; Zhang, S.-H.; Lim, S. H.; Liu, S.; Han, M.-Y. *Phys. Chem. Chem. Phys*. **2010**, *12*, 11923.
19. Seo, S.-W.; Jo, H.-H.; Lee, K.; Park, T.-J. *Adv. Mater*. **2003**, *15*, 795.
20. Niederberger, M.; Garnweitner, G. *Chem. Eur. J*. **2006**, *12*, 7282.
21. Joo, J.; Kwon, S. G.; Yu, J. H.; Hyeon, T. *Adv. Mater*. **2005**, *17*, 1873.
22. Hong, Z. S.; Cao, Y.; Deng, J. F. *Mater. Lett*. **2002**, *52*, 34.
23. Han, S.-Y.; Herman, G. S.; Chang, C.-H. *J. Am. Chem. Soc*, **2011**, *133*, 5166.
24. Chong, E.; Chun, Y.-S.; Kim, S.-H.; Lee, S.-Y. *Journal of Electrical Engineering & Techonology* **2011**, *6*, 539.
25. Kim, M.-S.; Hwang, Y.-H.; Kim, S.; Guo, Z.; Moon, D.-I.; Choi, J.-M.; Seol, M.-L.; Bae, B.-S.; Choi, Y.-K. *Appl. Phys. Lett*. **2012**, *101*, 243503.
26. Lee, J.; Choi, O.; Sim, E. *J. Phys. Chem. Lett*. **2012**, *3*, 714.
27. Liu, Y.; Gibbs, M.; Puthussery, J.; Gaik, S.; Ihly, R.; Hillhouse, H. W.; Matt, L. *Nano Lett*. **2010**, *10*, 1960.
28. Talapin, D. V.; Murray, C. B. *Science* **2005**, *310*, 86.